

## LOOKING INTO THE HORSEHEAD

MARC W. POUND

Department of Astronomy, University of Maryland, College Park, MD 20742; mpound@astro.umd.edu

BO REIPURTH

Institute for Astronomy, University of Hawaii, 2680 Woodlawn Drive, Honolulu, HI 96822; reipurth@ifh.hawaii.edu

AND

JOHN BALLY

Center for Astrophysics and Space Astronomy, University of Colorado, Boulder, CO 80309; bally@casa.coloradu.edu

Received 2002 October 22; accepted 2002 December 17

### ABSTRACT

We present the first interferometric CO (1–0) map of the Horsehead Nebula, made with the Berkeley-Illinois-Maryland Association array. The map has an angular resolution of about  $10''$ , corresponding to about 0.02 pc. The CO form of the Horsehead closely matches its appearance in visible dust, with the CO emission dominated by a bright, thin ridge along its western side. The molecular cloud exhibits a pronounced velocity gradient of  $5 \text{ km s}^{-1} \text{ pc}^{-1}$  from the northeast to the southwest, with the southwestern portion being redshifted. The mass of the cloud is  $27 M_{\odot}$ . We find an unusual U-shaped feature aligned with the “horse’s nose” for which we discuss several interpretations. The northern portion of the U may trace a small outflow driven by the embedded young star B33-1. We discuss the formation, evolution, and ultimate fate of this well-known nebula.

*Key words:* ISM: clouds — ISM: globules — ISM: individual (Horsehead Nebula) — ISM: kinematics and dynamics — stars: formation

### 1. INTRODUCTION

The Horsehead is probably one of the best known objects in the sky. In curious contrast to its fame among the general public, the number of scientific studies of the Horsehead is very limited. With this paper, we attempt to study the structure and star-forming properties of the Horsehead at millimeter wavelengths and relate these observations to ancillary optical and infrared data.

The Horsehead is located near the belt stars of Orion in the H II region IC 434, which runs north-south as a bright rim along a ridge of molecular material. The first mention of this luminous region appears in Herschel (1811), who lists a “diffused milky nebulosity” as his object No. 25. The Horsehead was first identified and recorded by Harvard College Observatory staff member Williamina Paton Fleming on a plate taken in 1888 as part of the extensive Harvard photographic program (Waldee & Hazen 1990). Various photographs were published and discussed by Pickering (1895), Roberts (1903), Wolf (1903), Keeler (1908), Barnard (1913), Curtis (1918), and Duncan (1921), and it became increasingly evident that the Horsehead represents a real physical unit and not merely a void among the stars. Barnard (1913) writes:

In the east side of the well known nebulous stream that runs southward from  $\zeta$  Orionis is a very conspicuous black notch which is very sharply defined. . . . This object has not received the attention that it deserves. It seems to be looked upon as a rift or hole in the nebulosity. . . . I have made numerous photographs of it, and in the past winter gave a long exposure with the expressed purpose of showing more definitely the true form of the object. . . . Instead of an indentation, the almost complete outline of a dark object is shown projected against the bright nebulosity. The west side of it is very definite and sharp, while

the eastern limit is scarcely discernible, and is entirely lost in the enlargement. . . . A glance at the original would show that this is not a perforation in the nebula. It is clearly a dark body projected against, and breaking the continuity of, the brighter nebulosity.

In this statement of nearly 90 years ago, Barnard took a clear stand against the idea that this “dark marking” of the sky should be an absence of stars and without hesitation advocated the existence of a dark physical body between the stars. Subsequently, in the catalog of Barnard (1919), the Horsehead got the name B33 by which it is known today.

The first indication that the IC 434 and Horsehead region could be related to young stars came with the discovery of H $\alpha$  emission line stars in the general area by Haro & Moreno (1953), followed by the detection of variable stars in the same region by Mannino (1959). Subsequently more H $\alpha$  emission stars were found in the region by Wiramihardja et al. (1989).

The first young star within the Horsehead itself was discovered by Reipurth & Bouchet (1984) as an infrared source, B33-1 (=IRAS 05383–0228), surrounded by a small, optically visible, nebulous cavity at its northwestern rim. These authors presented an evolutionary scenario in which the Horsehead is seen as a higher density cloud core in the process of being excavated from a larger and more tenuous cloud by the photoevaporation and photoablation caused by the UV radiation from the massive star system  $\sigma$  Orionis further to the west. In this model, the Horsehead is in an early phase of becoming a Bok globule (Reipurth 1983).

The first early millimeter studies showing that the Horsehead is a strong source at millimeter wavelengths were reported by Stark & Bally (1982), Sandell et al. (1985), and Suzuki et al. (1987). Further observations of the region in CS, [C II], and CO were presented by Lada, Bally, & Stark (1991), Zhou et al. (1993), and Kramer, Stutzki, &

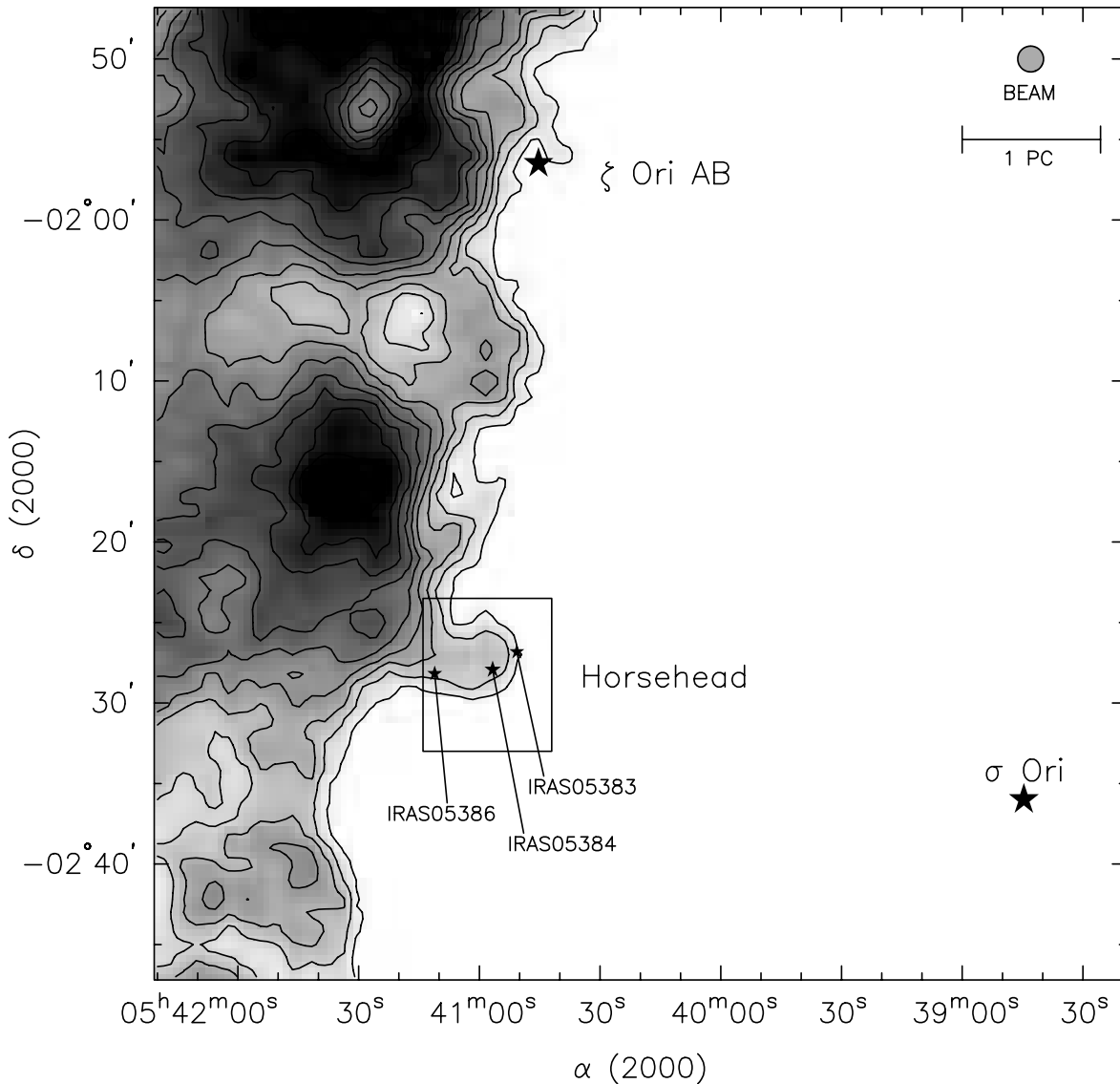


FIG. 1.—Large-scale map of CO (1–0) integrated intensity of part of the L1630 molecular cloud made with the Bell Labs 7 m telescope. The Horsehead is seen as an emission region extended out from the cloud edge. Location of nearby stars and *IRAS* sources are indicated (see Table 2 for full *IRAS* designations); the box shows the area mapped with BIMA. The gray scale ranges from 5 to 90 K km s<sup>-1</sup>; the contours are in steps of 10 K km s<sup>-1</sup>, starting at 10 K km s<sup>-1</sup>. The spectra were integrated between 8 and 12 km s<sup>-1</sup>.

Winnewisser (1996), respectively. [In the CS (2–1) map of Lada et. al, the Horsehead appears as clump 42.] A map of polarized starlight was presented by Zaritsky et al. (1987). Figure 1 is a large-scale CO (1–0) map from the Bell Labs Orion CO survey (Stark & Bally 1982; Bally et al. 1987; Bally, Langer, & Liu 1991; Miesch & Bally 1994) showing the location of the Horsehead in relation to the large L1630 cloud complex and with three embedded *IRAS* sources marked. Figure 2 is a wide-field CCD image of the Horsehead obtained at the KPNO 0.9 m telescope through an H $\alpha$  emission line filter. Features discussed in this paper are marked.

In this paper, we present millimeter interferometric maps of the Horsehead with high resolution. In § 2, we give details of our observational material. In § 3, we discuss the evidence for star formation in the Horsehead, followed by a presentation of our millimeter maps. In § 4, we interpret the millimeter data and discuss the evolutionary state and star forming properties of the Horsehead.

## 2. OBSERVATIONS

We mapped the Horsehead in the transition of <sup>12</sup>CO (1–0) at 115.271204 GHz with the Berkeley-Illinois-Maryland Association (BIMA) interferometer<sup>1</sup> during the 1998–2000 observing seasons. The BIMA array is a millimeter-wavelength interferometer located in Hat Creek, California (Welch et al. 1996), consisting of 10 6.1 m antennas. The nebula was observed with 29 mosaicked pointings on a hexagonal grid corresponding to Nyquist sampling of a 6.1 m antenna primary beam (100'' at 115 GHz) and covering a total area of about 5' × 6'. The pointing center was  $(\alpha, \delta)_{J2000.0} = (05^{\text{h}}41^{\text{m}}01^{\text{s}}.2,$

<sup>1</sup> The BIMA interferometer is operated under a joint agreement between the University of California, Berkeley, the University of Illinois, and the University of Maryland with support from the National Science Foundation.

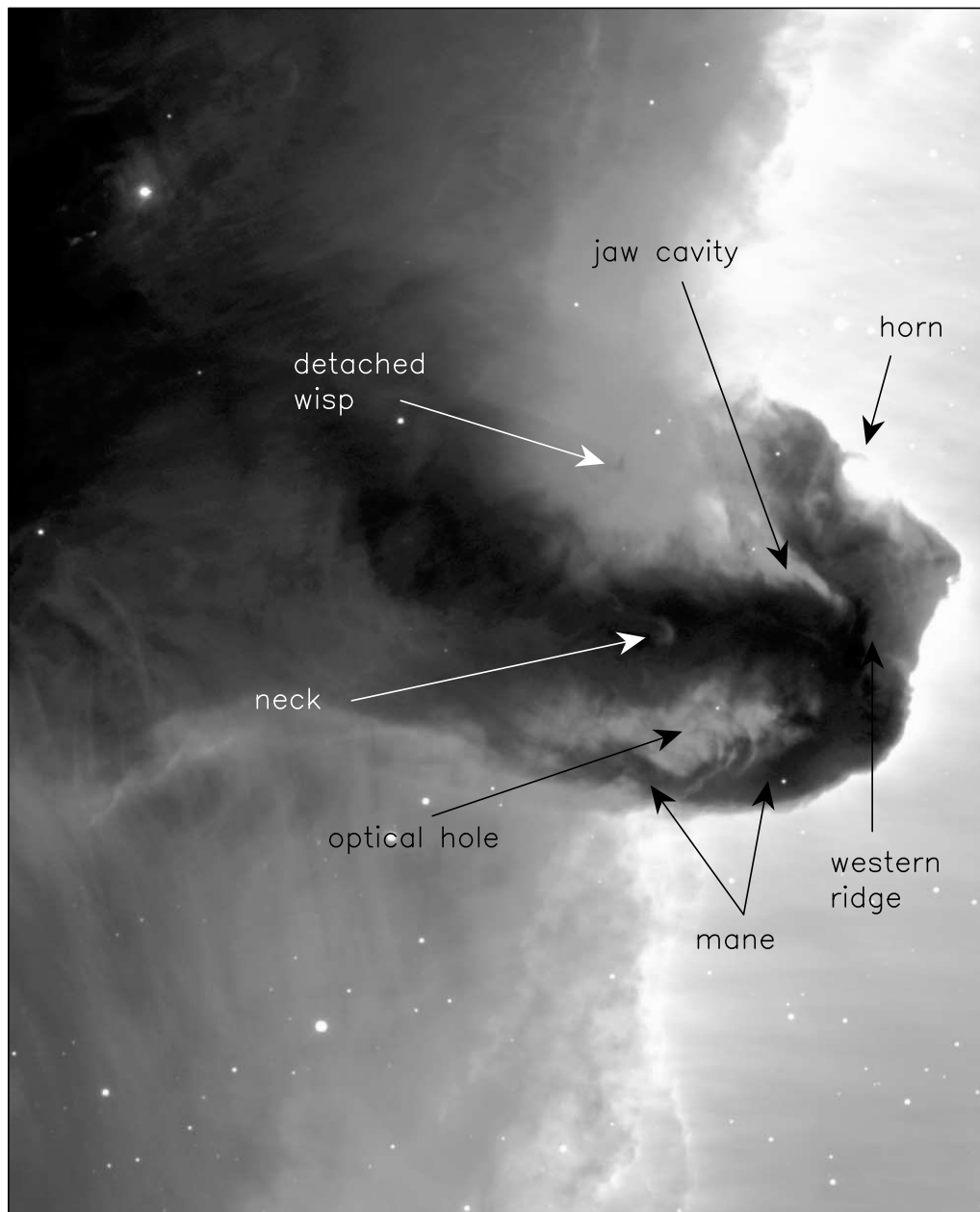


FIG. 2.—Wide-field CCD image of the Horsehead obtained through an  $H\alpha$  emission line filter. Features discussed in the text are marked. Image obtained at the 0.9 m KPNO telescope.

$-02^{\circ}28'12''.5$ ), with a velocity of  $9.0 \text{ km s}^{-1}$  with respect to the local standard of rest. We observed in both the C and D configurations of the array, sampling spatial frequencies from 1.6 to  $33 \text{ k}\lambda$ . The correlator contained a 25.0 MHz window with 256 channels to cover the  $^{12}\text{CO}$  (1–0) line in the upper sideband with a resolution of 0.1 MHz or  $0.26 \text{ km s}^{-1}$ . We simultaneously observed the transition of  $^{12}\text{C}^{17}\text{O}$  (1–0) at 112.35878 GHz in the lower sideband with identical spectral bandwidth and resolution and six continuum windows totalling 450 MHz. Typical single-sideband system temperatures ranged from 300 to 800 K. Absolute flux calibration was derived from observations of planets immediately before or after the source track. For tracks on successive days, we used the average calibration. The quasar 0530–135 was used as the phase

calibrator and secondary flux calibrator. The observations are summarized in Table 1.

Because the Horsehead is a large source compared with the interferometer primary beam, the interferometer may resolve out extended emission. Single-dish data are thus required to fill in the missing spatial frequency (the “zero spacing”). A fully sampled map of CO (1–0) covering the region imaged with the array was kindly obtained for us in 1999 December by Mark Heyer using the Five Colleges Radio Astronomy Observatory 14 m telescope, which has a  $45''$  FWHM beam at 115 GHz. These spectra have a typical rms noise of 0.2 K and identical velocity resolution as the BIMA data. A conversion from antenna temperature of  $43 \text{ Jy K}^{-1}$  (M. Heyer 1999, private communication) was applied to these data to put them on the same flux scale as

TABLE 1  
SUMMARY OF BIMA OBSERVATIONS

Date	Configuration	Flux Calibrator(s)	Derived 115 GHz Flux of 0530-135 (Jy)
1998 Nov 18 .....	C	Mars	$1.69 \pm 0.06$
1998 Nov 22 .....	C	Mars	$1.69 \pm 0.06$
1999 Mar 18 .....	D	Saturn	$2.44 \pm 0.05$
1999 Mar 19 .....	D	Saturn	$2.44 \pm 0.05$
1999 Apr 12 .....	C	Venus	$2.97 \pm 0.11$
1999 Apr 13 .....	C	Venus	$2.97 \pm 0.11$
1999 Aug 18 .....	D	Venus	$2.98 \pm 0.32$
1999 Sep 01 .....	D	Venus	$2.44 \pm 0.08$
2000 Apr 20 .....	C	Mars, 3C345	$2.48 \pm 0.09$
2000 Apr 26 .....	C	Mars, 3C345	$2.48 \pm 0.09$

the BIMA observations. The FCRAO map of CO integrated intensity,  $I(^{12}\text{CO})$ , is shown in Figure 3.

There are a variety of ways to combine single-dish and interferometric data. The “best” way depends on a host of variables such as source declination and morphology, relative flux in large- and small-scale features, S/N considerations,  $u$ - $v$  coverage, and relative sizes of the single-dish and interferometric antennas (Helfer et al. 2003). For our CO (1–0) data, we tried a number of different combination techniques and found that the method of Stanimirovic et al. (1999)—to linearly combine the single-dish and “dirty” interferometric maps, then jointly deconvolve them—produced the lowest residuals in the final map. The final synthesized beam size of the combined map (Fig. 4) is  $10''.4 \times 7''.6$ , corresponding to about 0.02 pc (4000 AU) at the 400 pc distance of the cloud (Lada et al. 1991). The  $1\sigma$  rms noise per channel in the final combined map is  $1.4 \text{ Jy beam}^{-1}$ . ( $1 \text{ Jy beam}^{-1} = 1.16 \text{ K}$  for this frequency and synthesized beam size).

We detected no  $^{12}\text{C}^{17}\text{O}$  (1–0) emission at a  $1\sigma$  rms level of  $0.5 \text{ Jy beam}^{-1}$  per channel, corresponding to  $1.1 \text{ Jy beam}^{-1} \text{ km s}^{-1}$  integrated between 9 and  $14 \text{ km s}^{-1}$ . No continuum emission was detected at an rms of  $150 \text{ mJy beam}^{-1}$ . These limits are derived solely from the interferometric data; no single-dish  $^{12}\text{C}^{17}\text{O}$  (1–0) or continuum observations were made.

### 3. RESULTS

#### 3.1. Evidence for Star Formation in the Horsehead

As noted in § 1, the clearest evidence for recent star formation is provided by the infrared source B33-1, which is located in a small nebulous cavity visible at the westernmost

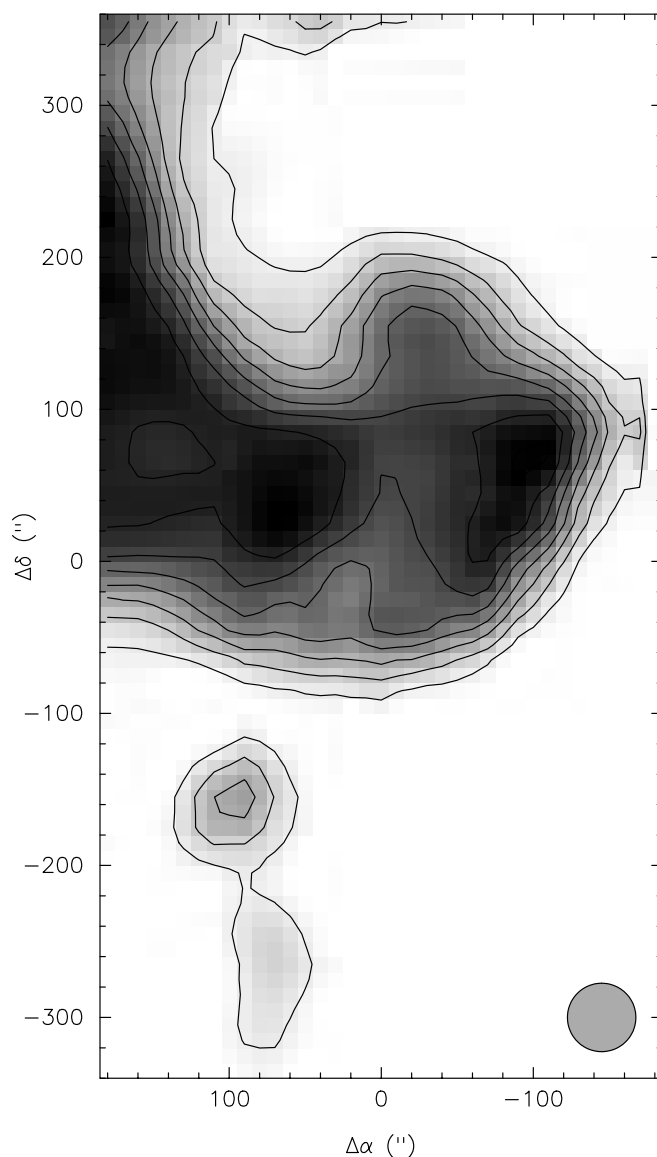


FIG. 3.—Integrated intensity of CO (1–0) between  $v_{\text{LSR}} = 8$  and  $15 \text{ km s}^{-1}$  made with the FCRAO 14 m telescope. These data were combined with the BIMA data to recover spatial frequencies resolved out by the interferometer (see Fig. 4). The gray scale ranges from 150 to  $900 \text{ Jy beam}^{-1} \text{ km s}^{-1}$ ; the contours are in steps of  $100 \text{ Jy beam}^{-1} \text{ km s}^{-1}$ , starting at  $200 \text{ Jy beam}^{-1} \text{ km s}^{-1}$ . The  $45''$  FWHM beam is indicated in the bottom right.

tip of the Horsehead (Reipurth & Bouchet 1984). This object coincides with the *IRAS* source 05383–0228. Subsequently, Sandell et al. (1985) noted the presence of two other *IRAS* sources toward the Horsehead (Table 2). *IRAS*

TABLE 2  
*IRAS* SOURCES TOWARD THE HORSEHEAD<sup>a</sup>

<i>IRAS</i>	$\alpha_{\text{B1950.0}}$	$\delta_{\text{B1950.0}}$	$F_{12}$	$F_{25}$	$F_{60}$	$F_{100}$
05383–0228 <sup>b</sup> .....	05 38 19.9	–02 28 19	0.48	1.30	(16.78L)	(137.85L)
05384–0229 .....	05 38 25.9	–02 29 15	(1.53L)	(2.21L)	(21.53L)	137.85
05386–0229 .....	05 38 40.3	–02 29 39	1.11	1.95	21.54:	(137.85L)

<sup>a</sup> Fluxes are in janskys.

<sup>b</sup> Also known as B33-1.

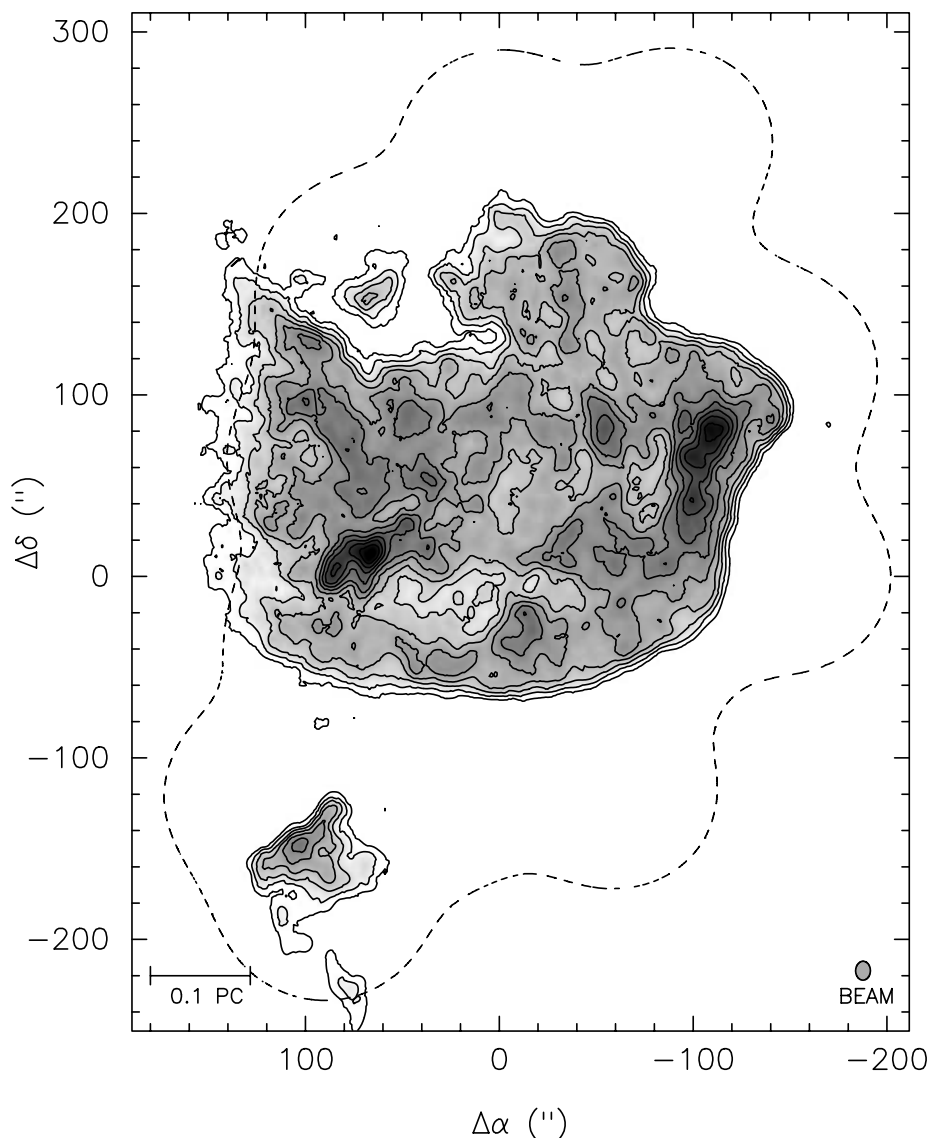


FIG. 4.—Combined FCRAO and BIMA CO map of the Horsehead. Details of the data combination are given in the text. The map shows CO integrated intensity between  $v_{\text{LSR}} = 8.25$  and  $14.25 \text{ km s}^{-1}$ . Contours are in steps of  $6 \text{ Jy beam}^{-1} \text{ km s}^{-1}$ , starting at  $6 \text{ Jy beam}^{-1} \text{ km s}^{-1}$ ; the gray scale ranges from 10 to  $65 \text{ Jy beam}^{-1} \text{ km s}^{-1}$ . Major features of the optical nebula are seen to have CO counterparts. The dashed line shows the mosaicked primary beam half-power point. The synthesized beam is indicated in the bottom right.

05384–0229 is detected at  $100 \mu\text{m}$  only and is located in the highly opaque southwest corner of the Horsehead. IRAS 05386–0229 is detected at 12, 25, and  $60 \mu\text{m}$  with a steeply rising energy distribution, suggesting a very young object; it is located at the very southeastern base of the Horsehead (see Fig. 1 and Table 2). It thus appears that at least three young stars have recently formed in the Horsehead.

Figure 5 shows the Horsehead in the recently released CCD images taken at the VLT.<sup>2</sup> The most unusual and characteristic feature, which has given rise to the name Horsehead, is the narrow, straight opening that begins the horse’s “jaw” and fans into a steadily widening cavity to the northeast. Reipurth & Bouchet (1984) claimed that part of this feature emits more strongly in [S II] and suggested that part of the emission in this region is due to a collimated

jet. This was contested by Neckel & Sarcander (1985), who used a brief long-slit spectrum to argue that the spectrum is purely one of an H II region. However, extracting spectra of faint, extinguished HH flows in bright H II regions is notoriously difficult, and the matter is not settled. Warren-Smith, Gledhill, & Scarrott (1985) used optical polarimetry to show that whatever component of reflected light there is in the cavity comes from the bright OB stars in the  $\sigma$  Orionis multiple system.

Reipurth & Bouchet (1984) speculated that a faint infrared source, B33-6, which is also optically visible as a faint star just beyond and southwest of the jaw (see Fig. 5), could be the driving source of the purported outflow. In light of what we have learned in the intervening years about outflow sources, this seems now highly unlikely. That *IRAS* has not detected a source near the beginning of the jaw suggests that, if it exists, it must be a very cool, deeply embedded source, perhaps of Class 0.

<sup>2</sup> Used by permission of the European Southern Observatory.

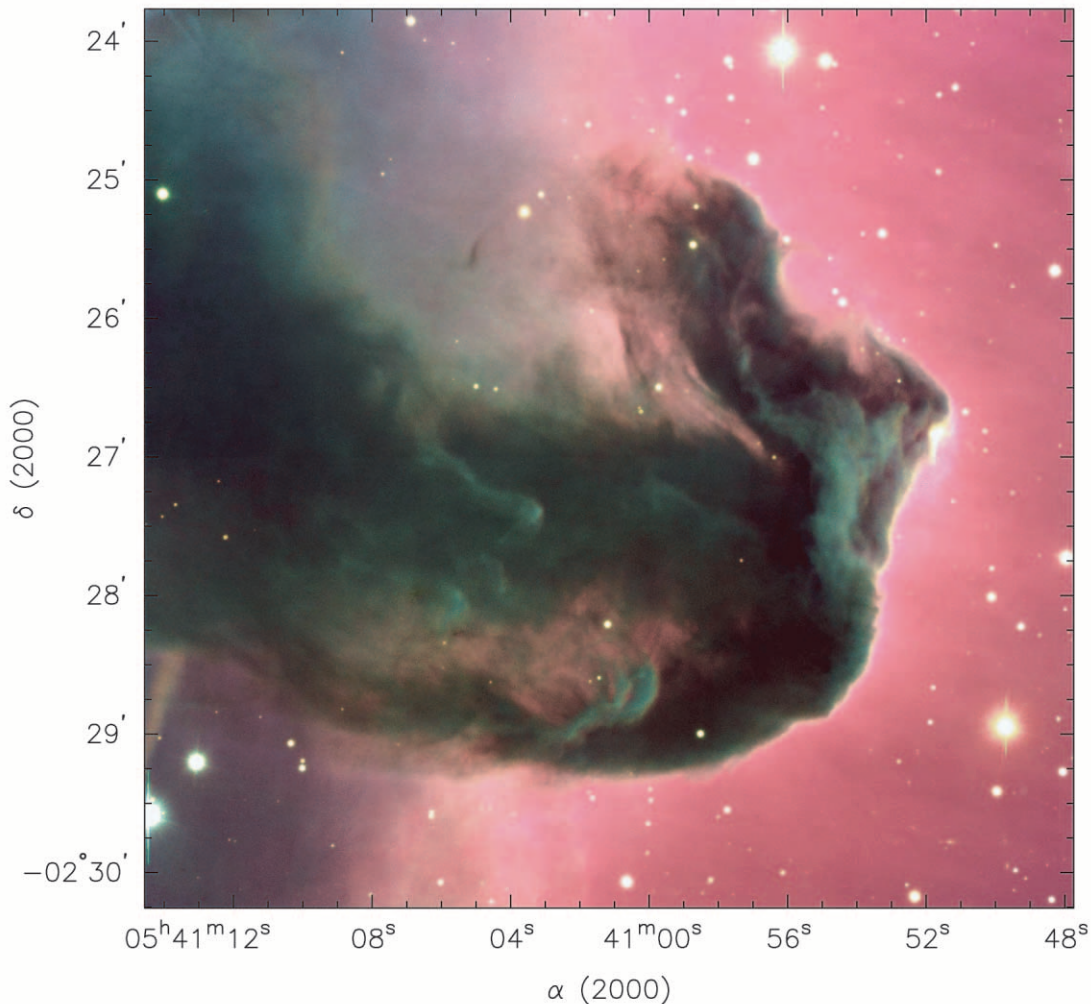


FIG. 5.—Composite color image of the Horsehead taken in the  $B$ ,  $V$ , and  $R$  bands with the VLT. The seeing in this image is about  $0''.75$ . Courtesy ESO.

Cavities similar to the jaw are rare, and therefore most probably represent a short-lived evolutionary phase. The high-resolution image in Figure 5 clearly shows structure and striations along the cavity axis, which suggest the effect of high-velocity gas on the dense gas in the globule. The closest similarity to the jaw is found in a southern Bok globule, Sa 136 or BHR 71, where the embedded source IRAS 11590–6452 has blown an outflow cavity with a quite similar optical morphology (e.g., Corporon & Reipurth 1997; Bourke 2001). In the following section, we demonstrate that the “jaw” closely coincides with a highly collimated CO feature.

### 3.2. BIMA Maps

#### 3.2.1. General Morphology

The first thing one notices about the CO map is that it has the classic equine shape from which the nebula gets its name. The CO contours “pile up” at the horse’s forehead, nose, and neck, indicating that those sides of the cloud have sharply defined edges. The cloud’s emission is dominated by a bright, thin ridge along and just inside its western edge. This ridge has a peak flux of  $62 \text{ Jy beam}^{-1} \text{ km s}^{-1}$ , more than twice the average brightness

of the rest of the cloud. The large optical hole in the horse’s neck appears as a dearth of CO emission, although the CO brightness is not zero there—some faint emission associated with the dust wisps threading the hole is visible, probably diluted in our beam. The denser, curving dust features near the western edge of the optical hole ( $\Delta\alpha, \Delta\delta \sim (-20'', -20'')$ ) have fairly bright CO emission centered at  $v_{\text{LSR}} \sim 10.25 \text{ km s}^{-1}$ . Three other bright ridges of emission are seen in the channel maps (Fig. 6). These are nearly perpendicular to the brightest ridge and lie along either side of the horse’s neck and along the north side of the optical hole. The isolated CO clump located just east of the horse’s nose corresponds to a detached wisp of dust seen in the optical images.

The bulk of CO emission from the Horsehead is confined to  $v_{\text{LSR}} = 9\text{--}12 \text{ km s}^{-1}$ . In both the channel maps and velocity-weighted moment map (Fig. 7), we can see that there is a velocity gradient from northeast to southwest. The magnitude of the velocity gradient is about  $5 \text{ km s}^{-1} \text{ pc}^{-1}$ , comparable to gradients seen in parts of the Eagle Nebula molecular cloud (Pound 1998). However, unlike the case of the Eagle Nebula, the direction of the velocity gradient does not appear to coincide with the direction to the exciting stars

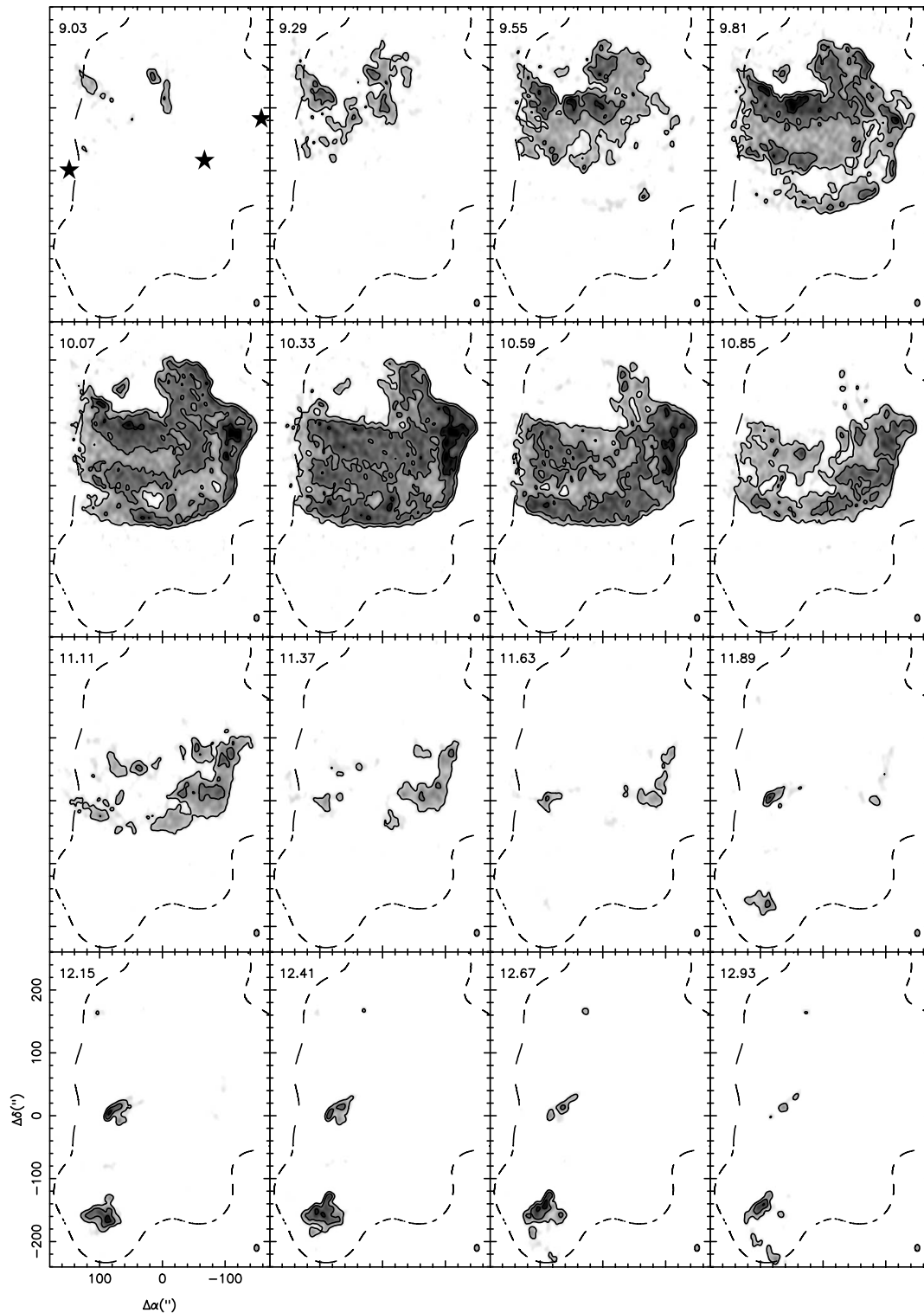


FIG. 6.—Individual CO channel maps of the combined data. In the first panel are indicated the positions of (from east to west) IRAS 05386, IRAS 05384, and IRAS 05383 (see Fig. 1 and Table 2). Contours are at intervals of  $5 \text{ Jy beam}^{-1}$  starting a  $10 \text{ Jy beam}^{-1}$ . The gray scale ranges from 5 to  $35 \text{ Jy beam}^{-1}$ . The dashed line shows the mosaicked primary beam half-power point. The synthesized beam is indicated in the bottom right of each panel.

in the  $\sigma$  Orionis system. A map of one-dimensional velocity dispersion is shown in the right panel of Figure 7. The dispersion is highest in the western ridge ( $\sigma_{v,\text{mean}} = 0.51 \pm 0.08 \text{ km s}^{-1}$ ,  $\sigma_{v,\text{max}} = 0.71 \text{ km s}^{-1}$ ) and neck regions ( $\sigma_{v,\text{mean}} = 0.47 \pm 0.06 \text{ km s}^{-1}$ ,  $\sigma_{v,\text{max}} = 0.68 \text{ km s}^{-1}$ ). In

creating the dispersion map, we masked out the compact sources directly behind the cloud (see § 3.2.3) to keep them from contaminating the dispersion calculation. They do not affect the velocity centroid map over the selected integration limits.

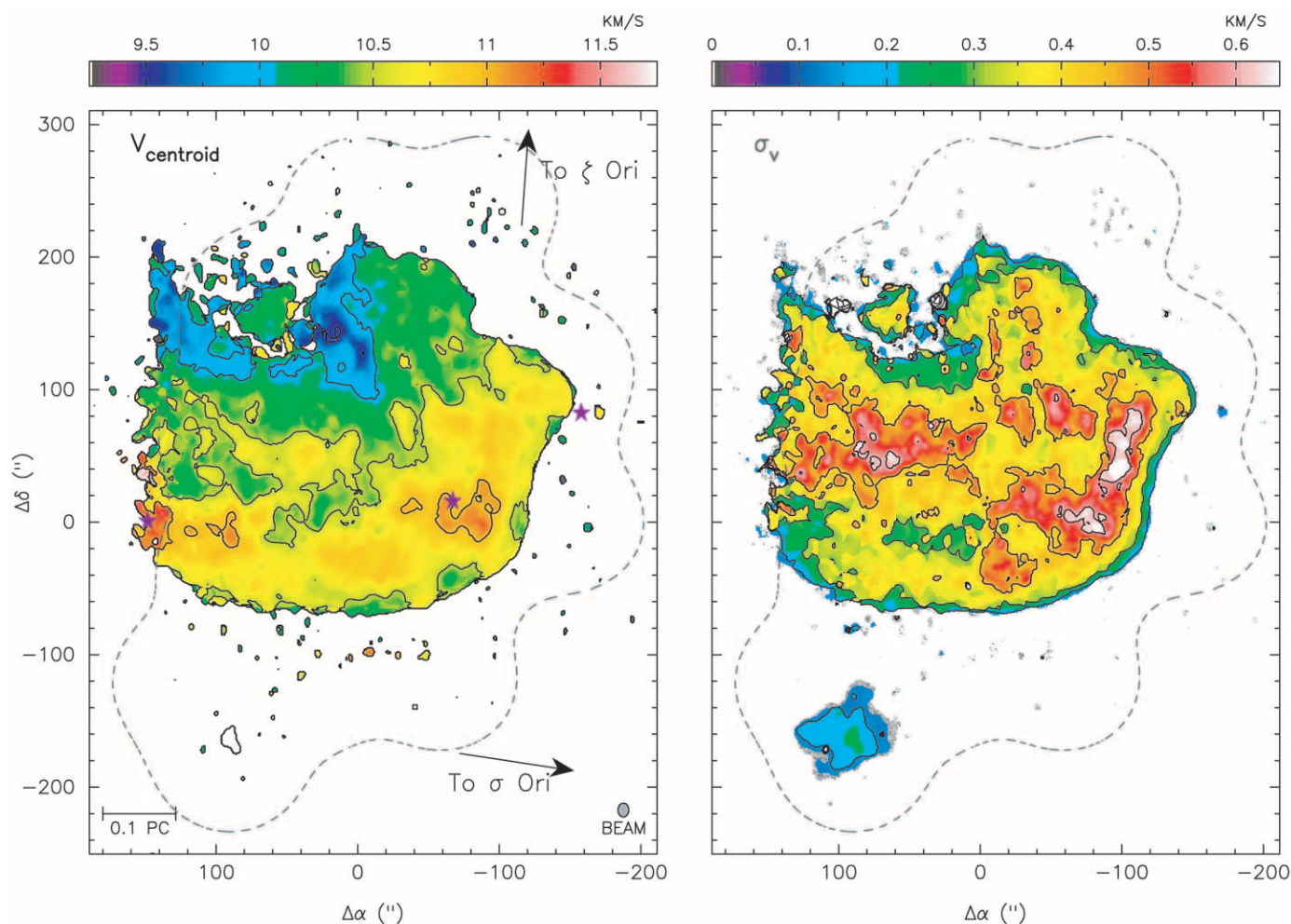


FIG. 7.—*Left*: Map of emission-weighted centroid velocity of CO computed between 9 and 12  $\text{km s}^{-1}$ . A systematic gradient across the face of the nebula is clearly evident. The magnitude of the gradient is about  $5 \text{ km s}^{-1} \text{ pc}^{-1}$ . Locations of *IRAS* sources are indicated with stars (see Fig. 1). Contours are in steps of  $0.5 \text{ km s}^{-1}$ . The dashed line shows the mosaicked primary beam half-power point. The synthesized beam is indicated in the bottom right. *Right*: Map of one-dimensional velocity dispersion,  $\sigma_v$ . See discussion in text.

### 3.2.2. Low-Velocity Features

We examined emission at velocities more negative than  $v_{\text{LSR}} = 8 \text{ km s}^{-1}$ , outside the velocity range of the main CO emission. Channel maps between  $v_{\text{LSR}} = 2.5$  and  $6.5 \text{ km s}^{-1}$  are shown in Figure 8, and CO integrated intensity between  $5.1$  and  $6.2 \text{ km s}^{-1}$  is shown in Figure 9. In these maps, we see a very intriguing U-shaped feature, with B33-1 at the apex and the southern leg directed along a line between B33-6 and the jaw opening. The northern leg of the U lies along the horse’s forehead, where it connects with a brighter patch of emission further north. We checked the single-dish maps for evidence of this U-shaped feature: the southern leg is clearly visible in the FCRAO channel maps, but the northern leg is confused with emission from a large clump in the background L1630 cloud.

The detailed correspondence between the CO and dust features is seen in Figure 10, a multicolor representation of the visible emission and CO emission from two velocity ranges. In the southern leg, the emission splits in two, following the edges of the jaw cavity extraordinarily well, coming together at the cavity’s apex. Further northeast

along the axis of the jaw cavity is the detached dust wisp described above, which is concave toward the jaw. In the northern leg, the emission follows along the edge of the horse’s forehead toward the curved “horn” seen in the optical, which seems to enclose a cavity. The CO emission fills the cavity, except for the region immediately around the stars B33-3 and B33-4 (see Reipurth & Bouchet 1984, their Fig. 1). In § 4.3, we discuss possible interpretations of these features.

Finally, we note the emission to the southeast extending from IRAS 05386 in the  $v_{\text{LSR}} = 4\text{--}5 \text{ km s}^{-1}$  range (Fig. 8). This feature coincides with a faint protuberance seen in the single-dish maps, but it has no clear counterpart in optical images.

### 3.2.3. Compact Sources

We find four compact sources at  $v_{\text{LSR}} \sim 13 \text{ km s}^{-1}$ , a more positive velocity than that of the Horsehead and the nearby L1630 cloud by about  $4\text{--}6 \text{ km s}^{-1}$  (Fig. 11). These show up as point sources in the FCRAO map, and the two brightest are also detected in the Bell Labs Orion CO survey. The brightest can also be seen faintly at CO (2–1) in the

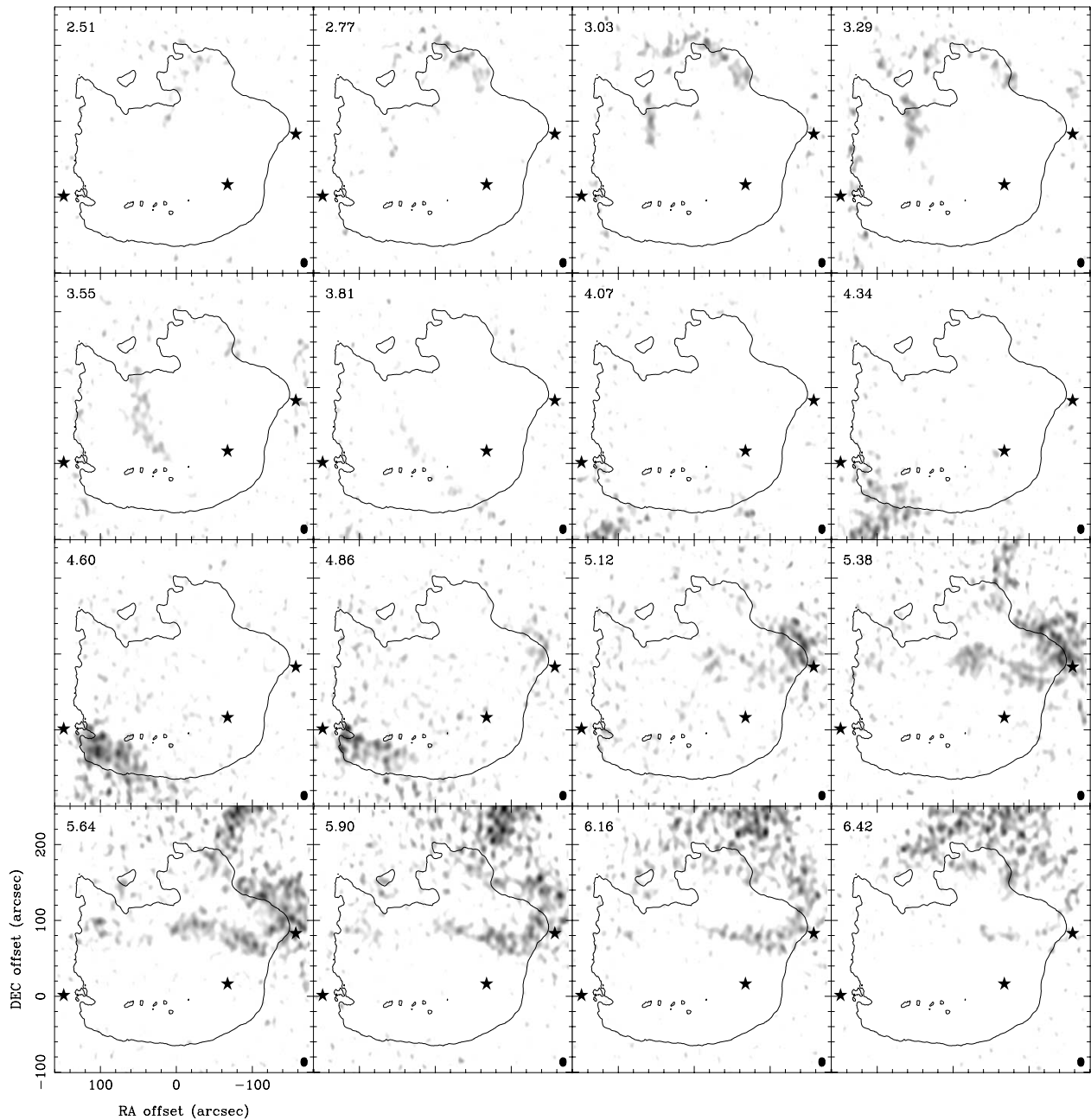


FIG. 8.—Individual CO channel maps of the combined data at velocities blueward of the main CO emission of the cloud. The U-shaped feature discussed in the text is visible in channels between 5 and 6.2 km s<sup>-1</sup>. The 15 Jy beam<sup>-1</sup> km s<sup>-1</sup> contour of the main CO emission (Fig. 4) is shown in the outline. Stars indicate the positions of the *IRAS* sources and B33-6. The gray scale ranges from 3 to 11 Jy beam<sup>-1</sup>. The synthesized beam is indicated in the bottom right of each panel.

spectral plots of Kramer et al. (1996). With the BIMA data, we can see more details of their structure. Source 1 (+100", -150") contains several smaller cores, a few of which appear elongated north-south. Source 2 (+75", +10") contains at least three cores and some extended emission northwest-southeast. Sources 3 (+30", +165") and 4 (+105", +162") lie just at the northern edge of the Horsehead and are unresolved by our observations. Source 4 appears slightly elongated northeast-southwest, and in the integrated map (Fig. 4) shows up as a small “tongue” of emission near the “horse’s mouth.” The positions of these sources do not correspond to any of the known IR sources, nor are they apparent as isolated dust clouds in visible images. Source 1

coincides with faint, extended dust emission in the 850  $\mu$ m map of Sandell et al. (2001).

#### 3.2.4. Mass Estimates

The Horsehead’s simple, predominantly Gaussian CO line profile shows that the nebula is a distinct, coherent object in velocity, as well as position, rather than a superposition of independent clouds. The average FWHM line width in the cloud is 1.5 km s<sup>-1</sup>. For a radius of 0.3 pc, this gives a gravitational mass of 43  $M_{\odot}$ , using equation (4) of Pound & Blitz (1993). Assuming a  $I(\text{CO})/N(\text{H}_2) = 2.5 \times 10^{20}$  K km s<sup>-1</sup> cm<sup>-2</sup>, we derive a luminous

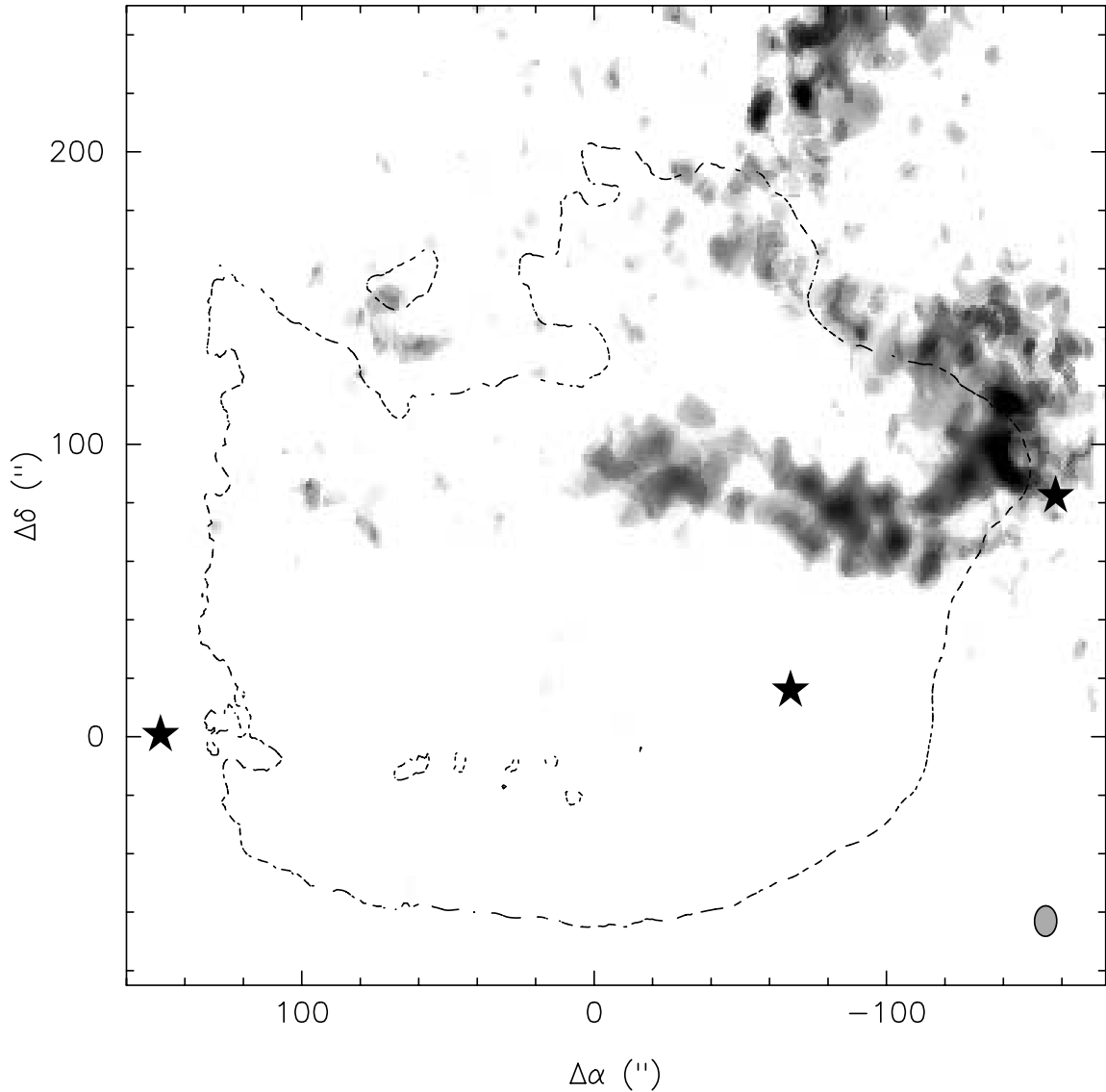


FIG. 9.—Map of the Horsehead “U” feature. Shown is  $I(^{12}\text{CO})$  between  $v_{\text{LSR}} = 5.1$  and  $6.2 \text{ km s}^{-1}$ , with the gray scale ranging from 2 to  $9 \text{ Jy beam}^{-1} \text{ km s}^{-1}$ . Three possible interpretations of this feature are discussed in the text. The patch of emission at  $(-80'', +230'')$  is part of the L1630 cloud in the background. As in previous figures, stars indicate infrared sources, solid outline is the  $15 \text{ Jy beam}^{-1} \text{ km s}^{-1}$  contour of Fig. 4, and the beam is in the bottom right.

mass  $M(\text{H}_2) \approx 27 M_{\odot}$  from the integrated intensity map in Figure 4. This leads to an average number density  $n(\text{H}_2) \approx 4800 \text{ cm}^{-3}$ . Similarly, the derived luminous masses of sources 1 through 4 are 1.3, 0.4, 0.03, and  $0.04 M_{\odot}$ , respectively.

#### 4. DISCUSSION

In this section, we discuss plausible scenarios for the formation and evolution of the Horsehead and explore the origins of the low-velocity U-shaped CO discussed above.

##### 4.1. Formation and Evolution of the Horsehead

The Horsehead may be similar to the tongues of dense gas that protrude into the interiors of many H II regions such as the famous “pillars” in M16 (Hester et al. 1996). (These are sometimes called elephant trunks, but we resist multiple animal metaphors!) However, unlike the M16

objects, which are cloaked in a brightly glowing photoionized skin, the Horsehead is seen predominantly in silhouette against the background plasma in IC 434, indicating that it is mostly illuminated on its back side.

Proposed formation mechanisms for such pillars generally fall into two broad categories: (1) instabilities at the boundary between the cloud and the ionized region that grow with time and (2) preexisting density enhancements (i.e., clumps) that locally retard the ionization front. Examples of pillar formation by instability are ablative Rayleigh-Taylor (RT) instability (Spitzer 1954; Frieman 1954; Kane et al. 2001), the shadowing instability (Williams 1999; Williams, Ward-Thompson, & Whitworth 2001), and the tilted radiation instability (Vandervoort 1962; Ryutov et al. 2003). The dense core scenario (Reipurth 1983) relies on the fact that the propagation speed of an ionization front depends inversely on the density of the medium. Thus, as an ionization front overruns a density inhomogeneity, a pillar can form. The front wraps around the condensation, its



FIG. 10.—Multicolor composite image showing the optical VLT image,  $I(^{12}\text{CO})$  in the U ( $v_{\text{LSR}} = 5.1\text{--}6.2 \text{ km s}^{-1}$ ; blue), and  $I(^{12}\text{CO})$  in the main cloud ( $v_{\text{LSR}} = 9\text{--}12 \text{ km s}^{-1}$ ; purple). The southern leg of the U bifurcates, following closely the outline of the jaw. The northern leg extends from B33-1 along the nose, with emission filling the horn cavity. The main emission matches well the dust morphology of the cloud.

propagation speed drops, and the front lags behind, forming a protrusion that points roughly toward the source of the ionizing radiation. The convergent pressure can increase the clump density further and, in some cases, may lead to radiation-driven implosion that can result in star formation (Bertoldi & McKee 1990).

It is remarkable that in many of these scenarios, the formation timescales are the same: a few hundred thousand years. In hydrodynamic simulations, the RT and shadowing instabilities give rise to 0.5 pc long protrusions in just over  $10^5$  yr. For the dense core mechanism, the formation timescale for a pillar is given by  $t_{\text{form}}(\text{yr}) \sim (5 \times 10^5) X_{0.5} \Delta V_{\text{kms}}$ , where  $X_{0.5}$  is the length of the protrusion in units of 0.5 pc, and  $\Delta V_{\text{kms}}$  is the difference between the propagation speed of the ionization front in the clump and in the surrounding lower density medium in units of  $1 \text{ km s}^{-1}$  (see also case IV

of Williams et al. 2001). This timescale is comparable to that required for the formation of a low-mass young stellar object. Thus, it is possible that the infrared sources embedded in the Horsehead are examples of triggered star formation. However, it is also possible that these sources, and their surrounding dense envelopes, predate the formation of the Horsehead. More precise age determinations than currently available for dating young stars are needed to determine which possibility is correct.

In the following, we consider how the detailed morphology and kinematics of the Horsehead may result from the interaction of the ionization front with the dense gas. The jaw cavity and the optical hole in the visual wavelength images of the Horsehead surround the opaque “neck” of dust that extends from the Orion B molecular cloud to the top of the horse’s head. The dust that makes up the “nose”

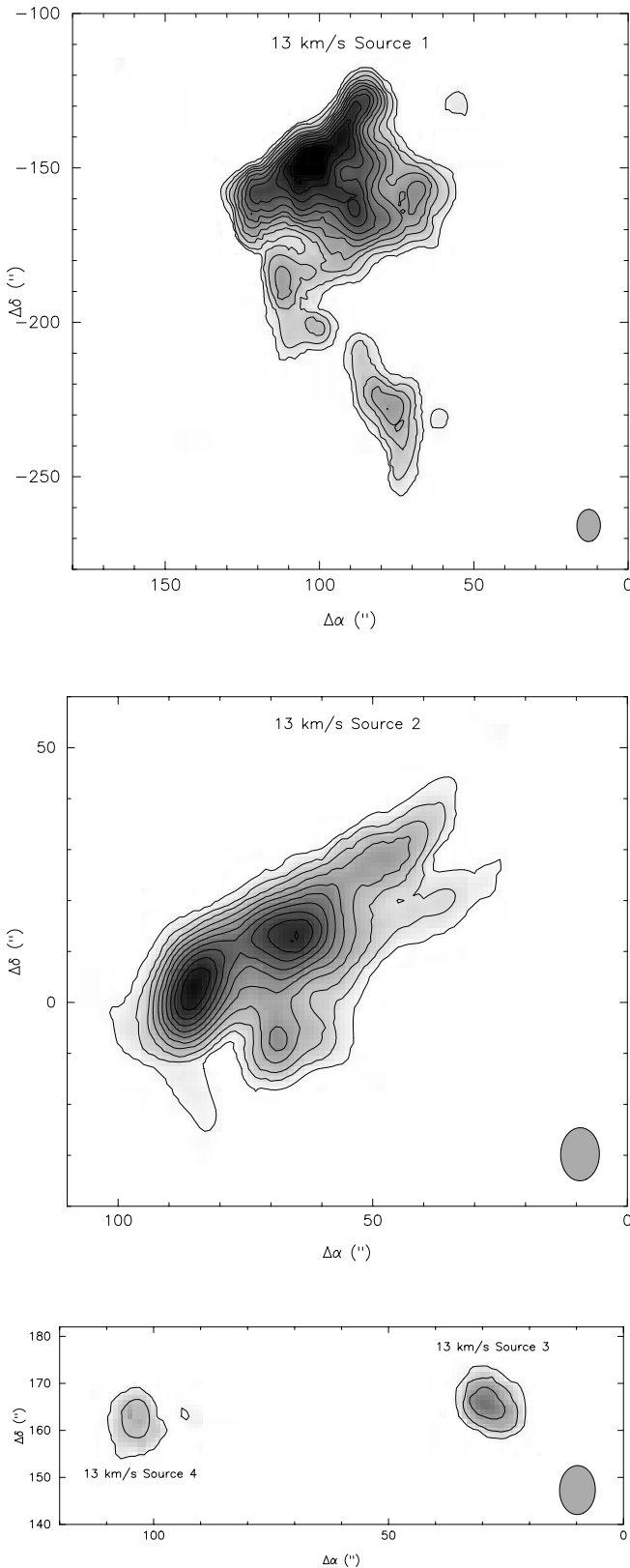


FIG. 11.—Maps of four compact sources found at  $v_{\text{LSR}} = 13 \text{ km s}^{-1}$ : (a) source 1; (b) source 2; (c) sources 3 and 4. These are probably not embedded in the Horsehead, since their centroid velocities are  $4 \text{ km s}^{-1}$  more positive than that of the nebula. Contours are integrated intensity between  $12.2$  and  $14 \text{ km s}^{-1}$  in steps of  $3 \text{ Jy beam}^{-1} \text{ km s}^{-1}$ , starting at  $3 \text{ Jy beam}^{-1} \text{ km s}^{-1}$ ; the gray scale ranges from  $2$  to  $35 \text{ Jy beam}^{-1} \text{ km s}^{-1}$  for sources 1 and 2 and from  $2$  to  $20 \text{ Jy beam}^{-1} \text{ km s}^{-1}$  for sources 3 and 4. The synthesized beam is indicated in the bottom right of each panel. For the relative locations of these sources, see Fig. 6.

and the “mane” look like a sheath of dense gas that has wrapped around the neck. The channel maps (Fig. 6) and centroid velocity diagram (Fig. 7) show that some portions of the gas at the edge of the Horsehead are redshifted with respect to the neck, while others are blueshifted. The neck can be traced from roughly  $v_{\text{LSR}} = 9.55$  to  $10.85 \text{ km s}^{-1}$ , while the western ridge and the mane extend from  $9.81$  to  $11.63 \text{ km s}^{-1}$ . From the centroid velocity diagram, we see that the CO emission within  $20''$ – $40''$  of the cloud’s western and southwestern edges become blueshifted by about  $0.3$ – $1 \text{ km s}^{-1}$  with respect to the western ridge and mane. The mane that wraps around the southern rim of the Horsehead is slightly redshifted with respect to the neck. On the other hand, the nose is seen predominantly on the blueshifted side of the neck from  $v_{\text{LSR}} = 9.29$  to  $10.59 \text{ km s}^{-1}$ .

Although these velocity differences are subtle, they demonstrate that the neck and the surrounding dust and associated CO have different kinematics. The mane, western ridge, and nose features can be interpreted as portions of the Horsehead that have been accelerated and wrapped around the neck by the propagating ionization front. Thus, these features may trace the dense gas behind the D-type shock front driven into the protrusion by the ionization front.

The kinematics of the mane and parts of the western ridge are difficult to reconcile with the fact that the nebula is seen mostly in silhouette, which indicates that it is backlit by  $\sigma$  Orionis. This geometry requires that the gas accelerated by the rocket effect be blueshifted rather than redshifted. Furthermore, the direction of the velocity gradient is not exactly toward  $\sigma$  Orionis, but skewed by some  $40^\circ$  toward the south. These details may indicate a preexisting velocity gradient in the cloud superposed on the rocket effect velocities. Another possibility is acceleration by a star in the foreground that has evolved off the main sequence.

The Horsehead is being evaporated by the UV radiation field of  $\sigma$  Orionis. We can estimate the evaporation time-scale,  $t_{\text{ev}}$ , by dividing the mass of the Horsehead by the mass-loss rate due to photoionization, which is approximately given by  $\dot{M} = 2\pi r_c^2 c_i m_p n_i$ , where  $c_i$  and  $n_i$  are the thermal sound speed and density in the ionized gas, respectively,  $m_p$  is the proton mass, and  $r_c$  is the radius of curvature of the cloud. The density of the plasma at the ionization front can be estimated by assuming that the Lyman continuum radiation field is absorbed in a layer with a thickness comparable to the radius of the cloud. Thus,  $n_i = (L_{\text{LyC}}/4\pi\alpha_B)^{1/2} r_c^{-1/2} d^{-1}$ , where the case B recombination coefficient is  $\alpha_B = 2.6 \times 10^{-13} \text{ cm}^3 \text{ s}^{-1}$  (Osterbrock 1989) and  $d$  is the distance from the Horsehead to  $\sigma$  Orionis. The spectral type of  $\sigma$  Orionis A is O9.5 V (Conti & Altshuler 1971); therefore, the star has a  $L_{\text{LyC}}$  of  $1.2 \times 10^{48} \text{ s}^{-1}$  (Panagia 1973). For  $d = 4 \text{ pc}$  and  $r_c = 0.2 \text{ pc}$ , we find  $n_i = 60 \text{ cm}^{-3}$ . This density is consistent with the  $\text{H}\alpha$  emission measure in the vicinity of the Horsehead. Thus, for  $c_i = 10 \text{ km s}^{-1}$ , the survival time of the Horsehead is about  $t_{\text{ev}} = M/\dot{M} \sim 5 \times 10^6 \text{ yr}$ .

#### 4.2. The Origin of the Horsehead’s Shape

The morphology of the Horsehead is that of a dense pillar protruding westward from the Orion B cloud (the neck) with a wide ridge of opaque material bent back toward Orion B, forming the nose, mane, and the gaps of the jaw cavity and the optical hole. This striking shape must have its

origin in physical processes, and here we explore the possibilities.

We cannot appeal to asymmetric radiation flux by multiple stars, since  $\sigma$  Orionis A appears to be the only significant nearby star. Nor can we invoke the Kelvin-Helmholtz (KH) vortices<sup>3</sup> that often accompany growing RT spikes in both scaled astrophysical laboratory simulations (Glendinning et al. 2000; Drake et al. 2002) and hydrodynamic simulations (Kane et al. 2001). The KH instability is suppressed when the pillar density is significantly higher than that of the ambient medium (i.e., when the Atwood number approaches one; see Richtmyer 1960), as is surely the case for the Horsehead.

The nose and mane can be explained if the original pillar already had some nonaxisymmetry, for instance, a head that was wider than the rest of the pillar, or embedded substructure. As ionization drove a D-type front into the western end of the feature, a dense globule of gas formed. Because the pillar head was asymmetric, material was pushed out on either side. Continued ablation pressure caused this sheet to wrap around the pillar, forming the shape we see today. Part of the dense globule may have suffered gravitational collapse to form the YSO B33-1, and the nose was further sculpted by an outflow therefrom. This picture requires the initial pillar (and thus the current cloud) to be thinner along the line of sight than it is wide. That is, the “neck” must have a roughly oval cross-section. If it were fully axisymmetric, then the wrapping sheet would obscure the horse’s neck, which we can plainly see.

#### 4.3. Possible Interpretations of the “U” Feature

We have come up with three possible interpretations of the U-shaped feature between 5.1 and 6.2 km s<sup>-1</sup> discussed in § 3.2.2, all of which have some merit, but none of which are completely satisfactory.

*Outflow(s).*—The U appears to be aligned with the dust features marking the jaw cavity and filaments, the horn and its enclosed cavity, and the detached wisp. It is possible that these features trace outflow activity from young stars embedded within the Horsehead. Because of its width (30,000 AU), it is very unlikely that the U is a single outflow, unless very old (Lee et al. 2002). Furthermore, if the edges of a single outflow lobe form the U, high-velocity gas is expected to fill the interior cavity. There is no evidence for such gas in either the CO or optical data. The best candidate for a genuine outflow is the northern leg of the U because of its association with B33-1 and the horn cavity. The CO emission here appears closely correlated with the optical dust morphology. The feature points directly toward the source B33-1 whose reflection nebula indicates that it is embedded within the Horsehead.

The southern leg—which notably lies almost exactly where Reipurth & Bouchet (1984) suggested that an outflow could have carved the jaw—traces the edges of the jaw cavity extremely well. The CO lobe tracing the edges has a narrow opening angle, suggesting a young outflow. The jaw

opening also contains many fine dust filaments along its length, suggesting streaming motion. However, the lobe does not have a known exciting source; any such source would have to be deeply embedded somewhere in the dense western ridge and probably be of Class 0. We note that the 850  $\mu$ m map of

Sandell et al. (2001) shows bright emission coincident with the western CO ridge.

There are problems, however, with the outflow interpretation. First, the U has no emission connecting it back in velocity space to the parent cloud. Thus, if the U-shaped feature traces outflows, then these flows have lobes that are detached from the parent cloud in velocity, an extremely unusual morphology for outflows. Second, while the northern leg of the U exhibits a velocity gradient, as is often seen in outflows, the southern leg does not (Fig. 12). Third, as noted above, the southern rim of the U does not appear to have a good candidate outflow source. Fourth, the outflow would be lacking a counterlobe (although this could be because it would run out the dense core).

*“Blow through”.*—The exciting star system  $\sigma$  Orionis is behind and to the southwest of the Horsehead cloud. It may be that molecular material, either from the L1630 cloud or from the far side of the Horsehead itself, has been swept up in the winds from these stars and is “blowing through” the jaw opening and around the top of the nose toward us. This would explain why the U is blueshifted with respect to the rest of the cloud. If this wind entrained some of the material in the jaw itself, it could also explain why the southern leg of the U traces the edges of the jaw so well. We do not see such emission around the southern and western edges of the Horsehead nor in the optical hole because very little background cloud emission exists toward these regions. However, this interpretation does not explain the existence of the horn and its cavity.

*Unrelated emission.*—The L1630 molecular cloud passes east-west behind the Horsehead, emitting at velocities  $V_{\text{LSR}} = 2$  to 7 km s<sup>-1</sup>, covering the range over which emission in the U is seen. Therefore, it is possible that the U is entirely unrelated to the Horsehead and due to source confusion along the line of sight. We view this possibility as unlikely. It would be a rather perverse coincidence if this unrelated feature just happened to line up with the horse’s nose and horn, just happened to have a known protostar at its apex, and just happened to trace the outline of the jaw in detail.

Finally, the U may be some combination of all three possibilities.

## 5. CONCLUSIONS

We present a mosaic of 29 interferometric CO maps of the Horsehead covering a 5'  $\times$  6' region with an angular resolution of about 10". The major results of this study are:

1. The mass of the Horsehead is 27  $M_{\odot}$ , and its CO emission is centered at  $v_{\text{LSR}} \approx 10$  km s<sup>-1</sup>. The Horsehead exhibits a pronounced velocity gradient of 5 km s<sup>-1</sup> pc<sup>-1</sup> from the northeast to the southwest, with the southwestern portion being redshifted. A fainter background cloud extends east-to-west behind the Horsehead at  $v_{\text{LSR}} \approx 6$  km s<sup>-1</sup>.

2. The CO form of the Horsehead closely matches that of the visual wavelength dust obscuration. The morphology consists of a dense east-west pillar that protrudes into the

<sup>3</sup> In the RT instability, as the growing pillar penetrates the lower density ambient medium, there is shear along the pillar sides, which triggers the KH instability. The KH instability causes perturbations to grow into vortex shapes, which creates the classic “mushroom” that one sees in RT simulations and experiments.

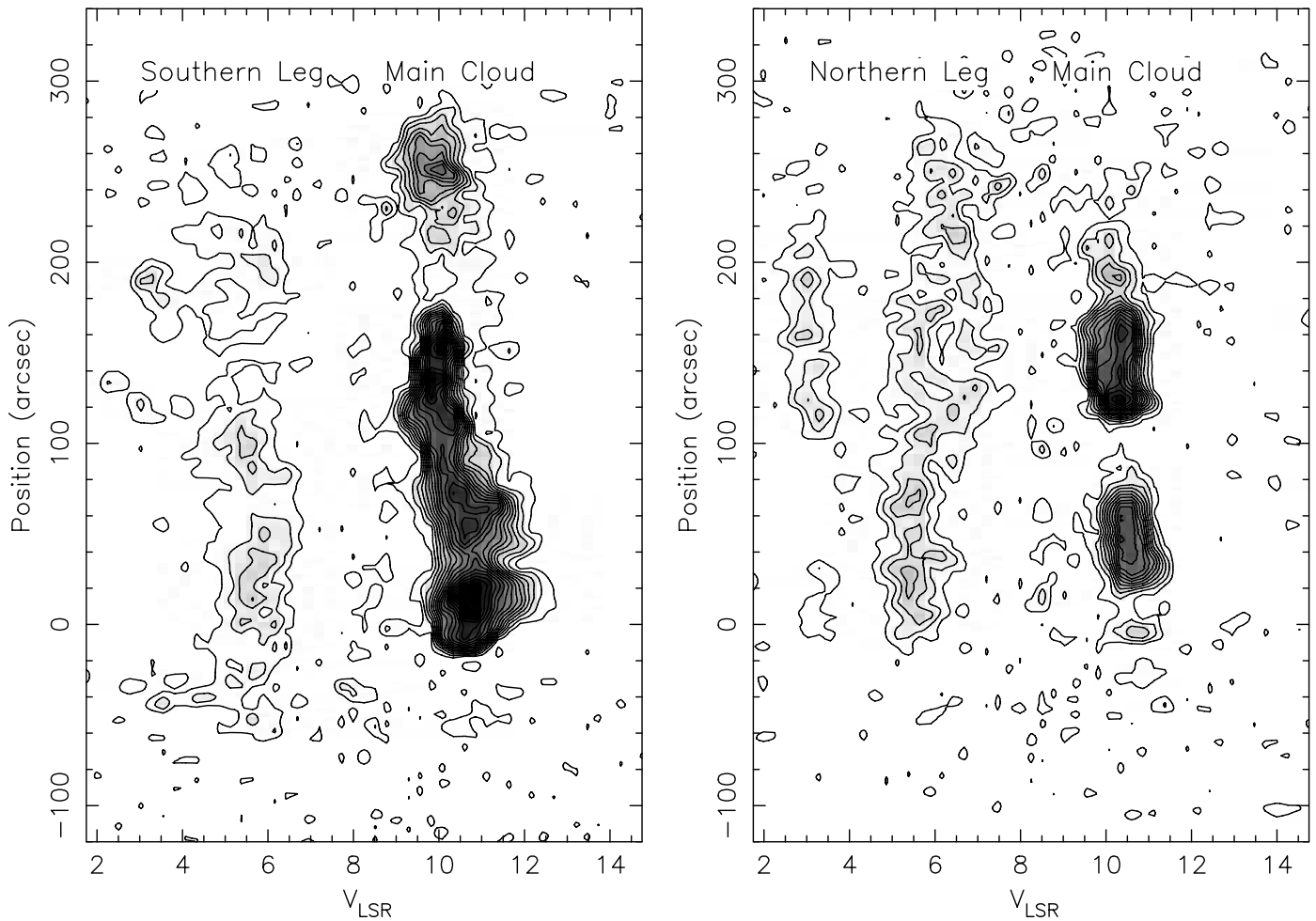


FIG. 12.—Position-velocity diagrams of the U feature that have been smoothed with a  $4''$  circular, Gaussian beam. Contours are in steps of  $2 \text{ Jy beam}^{-1}$  beginning at  $2 \text{ Jy beam}^{-1}$ ; the gray scale ranges from 3 to  $30 \text{ Jy beam}^{-1}$ . *Left*: Cut along the southern leg. *Right*: Cut along the northern leg.

IC 434 H II region. The pillar is surrounded by a dense ridge of gas that wraps around the western rim of the neck, forming the nose, western ridge, and mane of the Horsehead. This ridge has a slightly different velocity and larger velocity dispersion than the neck, indicating acceleration and turbulence.

3. A pair of cavities, namely the jaw lying between the nose and the neck and the optical hole lying between the mane and the neck, exist in the Horsehead. The jaw could be an outflow cavity, as previously suggested. Indeed, this feature is lined by a U-shaped pair of blueshifted CO filaments at  $v_{\text{LSR}} = 6 \text{ km s}^{-1}$ . The nature of these filaments is unknown. If they represent outflows, they are extremely unusual ones: they do not exhibit large velocity gradients and are disconnected in velocity from the parent cloud. The extended background cloud coincident in radial velocity further complicates the interpretation.

4. We consider two possible formation mechanisms for the Horsehead, by the work of an instability or by an ionization front. Both can produce a protrusion pointing toward the source of the UV radiation in the lower density surrounding medium. Each should have definite predictions for observed velocity fields, velocity dispersions, column densities, and temperature distributions. When detailed

hydrodynamic models are available, comparison to our data should be fruitful. The distinctive nose and mane of the horse may well have formed in response to ablative pressure on an initially asymmetric protrusion. If so, the “jaw cavity” and “optical hole” are then low-density regions between the relatively unperturbed neck and gas that has been wrapped around it.

5. The size of the Horsehead and its velocity gradient imply a formation timescale of order 0.5 Myr. The cloud is being photoablated; it is likely to be destroyed in about  $5 \times 10^6 \text{ yr}$ .

We thank Mark Heyer for obtaining the FCRAO data; Tamara Helfer and Mark Wolfire for helpful chats on deconvolution and photodissociation regions, respectively; and Travis Rector for help and advice in creating Figure 10. We are grateful to Göran Sandell for providing us with his  $850 \mu\text{m}$  map in advance of publication. M. W. P. extends special thanks to his Eagle project collaborators Jave Kane, Bruce Remington, Dmitri Ryutov, and Robin Williams for many stimulating discussions. BIMA observations at the University of Maryland are supported by the National Science Foundation through grant AST 99-81289.

## REFERENCES

- Bally, J., Langer, W. D., & Liu, W. 1991, *ApJ*, 383, 645  
 Bally, J., Stark, A. A., Wilson, R. W., & Langer, W. D. 1987, *ApJ*, 312, L45  
 Barnard, E. E. 1913, *ApJ*, 38, 496  
 ———. 1919, *ApJ*, 49, 1  
 Bertoldi, F., & McKee, C. F. 1990, *ApJ*, 354, 529  
 Bourke, T. L. 2001, *ApJ*, 554, L91  
 Conti, P. S., & Altshuler, W. R. 1971, *ApJ*, 170, 325  
 Corporon, P., & Reipurth, B. 1997, in *Poster Proc. IAU Symp.* 182, *Low Mass Star Formation—From Infall to Outflow*, ed. F. Malbet & A. Castets (Dordrecht: Kluwer), 85  
 Curtis, H. D. 1918, *PASP*, 30, 65  
 Drake, R. P., et al. 2002, *ApJ*, 564, 896  
 Duncan, J. C. 1921, *ApJ*, 53, 392  
 Frieman, E. A. 1954, *ApJ*, 120, 18  
 Glendinning, S. G., et al. 2000, *ApJS*, 127, 325  
 Haro, G., & Moreno, A. 1953, *Bol. Obs. Tonantzintla Tacubaya*, 1(7), 11  
 Helfer, T. T., Thornley, M. D., Regan, M. W., Wong, T., Sheth, K., Vogel, S. N., Blitz, L., & Bock, D. C.-J. 2003, *ApJ*, in press  
 Herschel, W. 1811, *Philos. Trans. R. Soc. London*, 101, 269  
 Hester, J. J., et al. 1996, *AJ*, 111, 2349  
 Kane, J. O., Ryutov, D. D., Remington, B. A., Glendinning, S. G., Pound, M. W., & Arnett, D. 2001, *BAAS*, 198, 64.05  
 Keeler, J. E. 1908, *Publ. Lick Obs.*, 8, 1  
 Kramer, C., Stutzki, J., & Winnewisser, G. 1996, *A&A*, 307, 915  
 Lada, E. A., Bally, J., & Stark, A. A. 1991, *ApJ*, 368, 432  
 Lee, C. F., Mundy, L. G., Stone, J. M., & Ostriker, E. C. 2002, *ApJ*, 576, 294  
 Mannino, G. 1959, *Pub. Oss. Astron. Bologna*, 7, No. 10  
 Miesch, M. S., & Bally, J. 1994, *ApJ*, 429, 645  
 Neckel, Th., & Sarcander, M. 1985, *A&A*, 147, L1  
 Osterbrock, D. E. 1989, *Astrophysics of Gaseous Nebulae and Active Galactic Nuclei* (Mill Valley: Univ. Sci.), 19  
 Panagia, N. 1973, *AJ*, 78, 929  
 Pickering, W. H. 1895, *Ann. Harvard Coll. Obs.*, 32, 66  
 Pound, M. W. 1998, *ApJ*, 493, L113  
 Pound, M. W., & Blitz, L. 1993, *ApJ*, 418, 328  
 Reipurth, B. 1983, *A&A*, 117, 183  
 Reipurth, B., & Bouchet, P. 1984, *A&A*, 137, L1  
 Richtmyer, R. D. 1960, *Commun. Pure Appl. Math.*, 13, 297  
 Roberts, I. 1903, *ApJ*, 17, 72  
 Ryutov, D. D., Kane, J. O., Pound, M. W., & Remington, B. A. 2003, *Plasma Phys. Controlled Fusion*, submitted  
 Sandell, G., Jenness, T., McMullin, J. P., & Shah, R. Y. 2001, *BAAS*, 199, 156.01  
 Sandell, G., Reipurth, B., Menten, K., Walmsley, C. M., & Ungerechts, H. 1985, in *Light on Dark Matter*, ed. F. P. Israel (Dordrecht: Reidel), 295  
 Spitzer, L. 1954, *ApJ*, 120, 1  
 Stanimirovic, S., Staveley-Smith, L., Dickey, J. M., Sault, R. J., & Snowden, S. L. 1999, *MNRAS*, 302, 417  
 Stark, A. A., & Bally, J. 1982, in *Regions of Recent Star Formation*, ed. R. S. Roger & P. E. Dewdney (Dordrecht: Reidel), 329  
 Suzuki, H., Kaifu, N., Ohishi, M., Miyaji, T., & Ishikawa, S. 1987, in *IAU Symp.* 115, *Star Forming Regions*, ed. M. Peimbert & J. Jugaku (Dordrecht: Reidel), 90  
 Vandervoort, P. O. 1962, *ApJ*, 135, 212  
 Waldee, S. R., & Hazen, M. L. 1990, *PASP*, 102, 1337  
 Warren-Smith, R. F., Gledhill, T. M., & Scarrott, S. M. 1985, *MNRAS*, 215, 75P  
 Welch, W. J., et al. 1996, *PASP*, 108, 93  
 Williams, R. J. R. 1999, *MNRAS*, 310, 789  
 Williams, R. J. R., Ward-Thompson, D., & Whitworth, A. P. 2001, *MNRAS*, 327, 788  
 Wiramihardja, S. D., Kogure, T., Yoshida, S., Ogura, K., & Nakano, M. 1989, *PASJ*, 41, 155  
 Wolf, M. 1903, *MNRAS*, 63, 303  
 Zaritsky, D., Shaya, E. J., Tytler, D., Scoville, N. Z., & Sargent, A. I. 1987, *AJ*, 93, 1514  
 Zhou, S., Jaffe, D. T., Howe, J. E., Geis, N., Herrmann, F., Madden, S. C., Poglitsch, A., & Stacey, G. J. 1993, *ApJ*, 419, 190

*Note added in proof.*—The following information was provided by Martha Hazen, former Curator of Astronomical Photographs at Harvard College Observatory:

Bache plate B2312 taken by Fleming is considered the discovery plate, but not the first plate, as it turns out. Plate B2312 shows the three bright stars of Orion's Belt and the Horsehead. The Henry brothers took a photograph of it at the Paris Observatory on 1887 Feb 28; B2312 was taken 1888 Feb 8. However, a search through Harvard College Observatory's plate collection uncovered two earlier Bache plates that record the Horsehead—B193 taken 1885 Dec 11, which shows the Horsehead quite clearly, and B1043 taken 1887 Jan 25, on which the Horsehead can be vaguely seen.